# Tip-Enhanced Raman Spectroscopy with Picosecond Pulses

**ARTICLE** *in* JOURNAL OF PHYSICAL CHEMISTRY LETTERS · DECEMBER 2013

Impact Factor: 7.46 · DOI: 10.1021/jz4024404



**4 AUTHORS**, INCLUDING:

Jordan M Klingsporn
Northwestern University
**12** PUBLICATIONS **297** CITATIONS
SEE PROFILE

Matthew D Sonntag
Albright College
**10** PUBLICATIONS **291** CITATIONS
SEE PROFILE

THE JOURNAL OF PHYSICAL CHEMISTRY Letters

Letter

pubs.acs.org/JPCL

# Tip-Enhanced Raman Spectroscopy with Picosecond Pulses

Jordan M. Klingsporn,[†] Matthew D. Sonntag,[†] Tamar Seideman, and Richard P. Van Duyne*

Northwestern University, Department of Chemistry, 2145 Sheridan Road, Evanston, Illinois 60208, United States

Supporting Information

**ABSTRACT:** Tip-enhanced Raman spectroscopy (TERS) can probe chemistry occurring at surfaces with both nanometer spectroscopic and submolecular spatial resolution. Combining ultrafast spectroscopy with TERS allows for picosecond and, in principle, femtosecond temporal resolution. Here we couple an optical parametric oscillator (OPO) with a scanning tunneling microscopy (STM)-TERS microscope to excite the tip plasmon with a picosecond excitation source. The plasmonic tip was not damaged with OPO excitation, and TER spectra were observed for two resonant adsorbates. The TERS signal under ultrafast pulsed excitation decays on the time scale of 10 s of seconds; whereas with continuous-wave excitation no decay occurs. An analysis of possible decay mechanisms and their temporal characteristics is given.

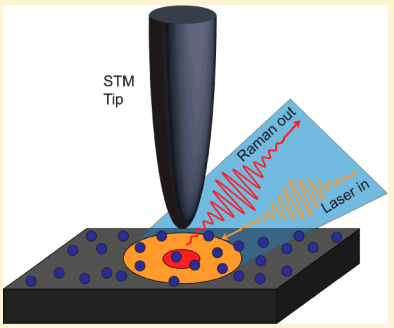


**SECTION:** Plasmonics, Optical Materials, and Hard Matter

Probing site-specific chemistry with high temporal resolution opens the field of tip-enhanced Raman spectroscopy (TERS) to new opportunities in areas such as catalysis, photovoltaics, plasmon-induced chemistry, single-molecule dynamics, coherent and incoherent laser control techniques, and hot photoelectron generation. TERS provides a promising technique for such studies, as it can probe spectroscopic information below the diffraction limit of light and provide submolecular resolution topographic information. However, monitoring chemistry and molecular dynamics at a surface also requires high temporal resolution, which cannot be achieved in TERS with continuous-wave (CW) excitation. Demonstrating that TERS can be performed with pulsed excitation sources is both a necessary and important step on the pathway to achieve the monitoring of reactions on the femto- to picosecond time scale with high spatial resolution and chemical sensitivity.

Recently, the field of TERS has produced a number of publications highlighting the strengths of this technique.[1−4] For instance, single-molecule sensitivity for TERS has been demonstrated at various levels of rigor.[5−9] In another exciting result, Zhang et al. have recently shown that spatial resolution below 1 nm can be achieved with TERS.[9] Zenobi and coworkers have explored other substrate materials including nonplasmonic materials and have shown how TERS signal intensity decreases by a factor of 10 with nonplasmonic substrates.[10] Additionally, TERS has been achieved in ultrahigh vacuum (UHV) environments.[6,9,11] Furthermore, there have been a number of results involving the coupling of ultrafast laser pulses into the tip−sample junction.[12−18] However, the majority of these cases involve studying photoelectron generation from the tip−sample junction, time-resolved STM, or second harmonic generation (SHG) of inorganic compounds and do not measure a molecularly specific signal or show plasmon-enhanced phenomena. For example, the Raschke group has developed a technique using a grating coupler on the tip to introduce ultrafast pulses to the tip−sample junction.[19] In one case, they used pulse shaping and feedback monitoring of the second harmonic response at the tip apex to control the optical waveform of the scattered light. One of the few examples of studying a molecular sample involved tip-enhanced coherent anti-Stokes Raman spectroscopy (TE-CARS). In these nonresonant experiments, no degradation of the Raman signal was observed despite maintaining high peak powers.[20,21] Because of the high peak powers focused at the tip−sample junction, both the tip and the substrate must be able to withstand the intense excitation source as well as the extremely high fields that are confined to the tip−sample junction. Several groups have reported morphological and spectral changes in metallic colloids and arrays upon exposure to femtosecond light.[22,23] Other groups using picosecond pulses have not observed any changes, spectrally or physically, upon irradiation of a plasmonic surface with power densities up to $1.3 \times 10^4$ W/cm$^2$.[24,25] It should be mentioned that these groups utilized excitation in the NIR regime. In one case, visible excitation at 532 nm was limited to $1.3 \times 10^2$ W/cm$^2$ to prevent sample degradation.[24] Nonetheless, there are several challenges that must be overcome to successfully combine ultrafast spectroscopy with TERS.

Herein we demonstrate the coupling of a picosecond optical parametric oscillator (OPO) with an ambient scanning tunneling microscopy (STM)-TERS microscope and show that it is possible to overcome several of the challenges involved with ultrafast TERS of resonant adsorbates. Malachite green isothiocyanate (MGITC) and crystal violet (CV) were studied because both of these dyes have large Raman cross sections

**Received:** November 12, 2013
**Accepted:** December 11, 2013
**Published:** December 11, 2013

  

with different adsorption properties. MGITC is covalently bound to the Ag surface, while CV is not; thus CV can freely diffuse on the Ag surface. The absorbance maximum of MGITC is located at $\lambda_{max}$ = 620 nm, while the absorbance maximum of CV is located at $\lambda_{max}$ = 590 nm (Figures S1 and S2 in the Supporting Information). Therefore, the 594 nm excitation light is strongly in resonance with the molecular transitions of both MGITC and CV. While this work overcomes several of the challenges of coupling ultrafast spectroscopy with TERS, signal decay of the molecules in the tip−sample junction must still be managed. This would allow TERS to achieve high temporal resolution along with nanometer spatial and submolecular topographic resolution, providing a powerful tool to study site-specific chemistry at concentrations down to the single-molecule level.

TERS spectra were reliably obtained for MGITC with picosecond excitation focused at the tip−sample junction. However, Figure 1A shows the MGITC TER signal decays over 50 s. No additional Raman lines or background signal appeared, indicating that MGITC is not decomposing. In CW experiments (Figure 1B,a), no time-dependent signal loss occurred (Figures S3 and S4 in the Supporting Information), indicating that the decay mechanism is related to the pulsed nature of the excitation. Figure 1B,a shows a TER spectrum obtained with CW excitation at similar average power is compared with a picosecond spectrum (Figure 1B,b) extracted from the waterfall plot. Figure 1B,c is a spectrum obtained by averaging over all spectra obtained under pulsed excitation. The peak positions line up well, as shown by the dashed lines, demonstrating that the dyes themselves are being observed. Additionally, the signal-to-noise in the pulsed experiment is similar to what is observed under CW excitation.

We further investigate the stability of the TER signal under picosecond excitation of the plasmonic tip−sample junction by examining a different molecule, CV. The tip is kept retracted from the sample for the first 60 s of the experiment, at which point it is brought into tunneling range and the TER signal appears. Similarly to MGITC, the peak positions and S/N match well with those observed in CW TERS. As can be seen in Figure 2A, the signal loss occurs roughly 40 s after the signal is first observed.

Measuring the enhancement factor in these situations is complicated by both the signal decay and the fact that no retracted signal is observed due to the low coverage used. Given that our tips are reproducible, we can provide an upper limit to the radius of curvature by scanning electron microscopy (SEM) examination. An estimate of the relative enhancement factor can be achieved by assuming that the far-field signal is just below the noise level, ∼400 ADU $mW^{-1}$ $s^{-1}$. Using the measured far-field focal spot size, engaged intensity, and the estimated tip enhancement area, the TERS enhancement factor (EF) is calculated using the following equation:

$$EF_{TERS} = \frac{I_{engaged} - I_{retracted}/R_{TERS}}{I_{retracted}/R_{background}} = \left(\frac{I_{engaged}}{I_{retracted}} - 1\right)\frac{R_{background}}{R_{TERS}}$$

Analysis of the intensity is straightforward; however, care must be taken in the calculation of the number of molecules probed in each case. Because of the larger laser spot size, the retracted signal originates from the number of molecules

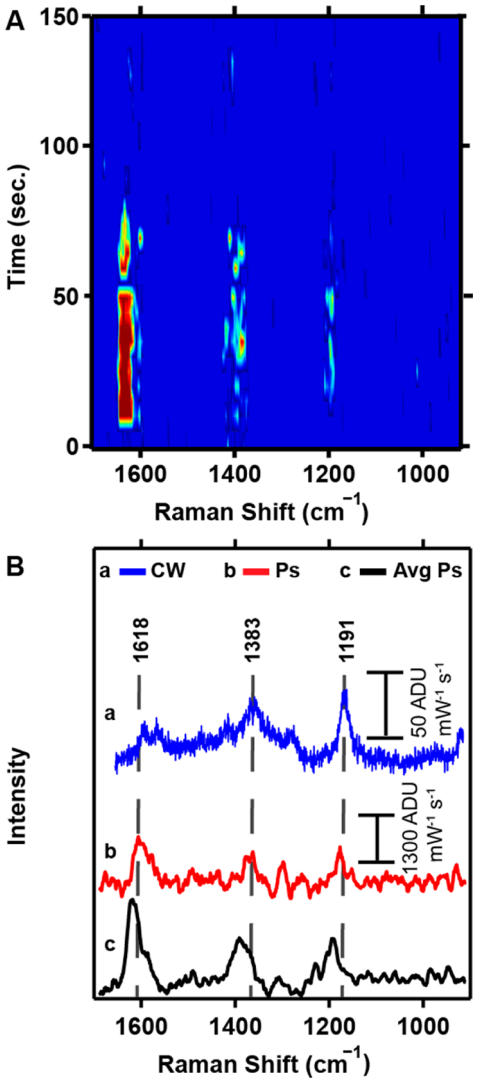


**Figure 1.** (A) Time series waterfall plot of MGITC, demonstrating disappearance of the TER signal under pulsed excitation. The disappearance occurs within 50 s. (B) Comparison of pulsed versus CW excitation. Ps TERS spectra acquired with $\lambda_{ex}$ = 594 nm, $t_{aq}$ = 5 s, and $P_{ex}$ = 30 W/cm$^2$ and tunneling conditions of 3 nA and 500 mV. CW TERS spectra acquired with $\lambda_{ex}$ = 594 nm, $t_{aq}$ = 5 s, and average $P_{ex}$ = $10^3$ W/cm$^2$.

contained within the laser focal area. The laser spot radius is 2 $\mu$m, and with monolayer coverage, we can use the areas probed for the engaged and retracted spectra to determine the EF. An STM tip radius of 150 nm leads to a tip-enhancing region with a radius of 75 nm.[26] The enhancement factor for the TERS spectrum of crystal violet was therefore calculated as 1.1 × $10^4$ based on the intensity of the 1594 $cm^{-1}$ peak, while the enhancement factor of MGITC is 1.4 × $10^4$ based on the intensity of the 1618 $cm^{-1}$ peak. As the signal immediately begins to decrease upon measurement and the retracted signal is below the noise limit, the EF values reported are the lowest possible consistent with the data.

In these experiments, the high field intensities generated in the plasmonic tip−sample junction could damage the tip, molecule, or both leading to the loss of signal. Typically, an average power density of ∼30 W/cm$^2$ was used, which is ∼30 times smaller than the typical ∼$10^3$ W/cm$^2$ used in CW experiments. However, the peak power density of ∼$10^5$ W/cm$^2$


dx.doi.org/10.1021/jz4024404 | J. Phys. Chem. Lett. 2014, 5, 106−110

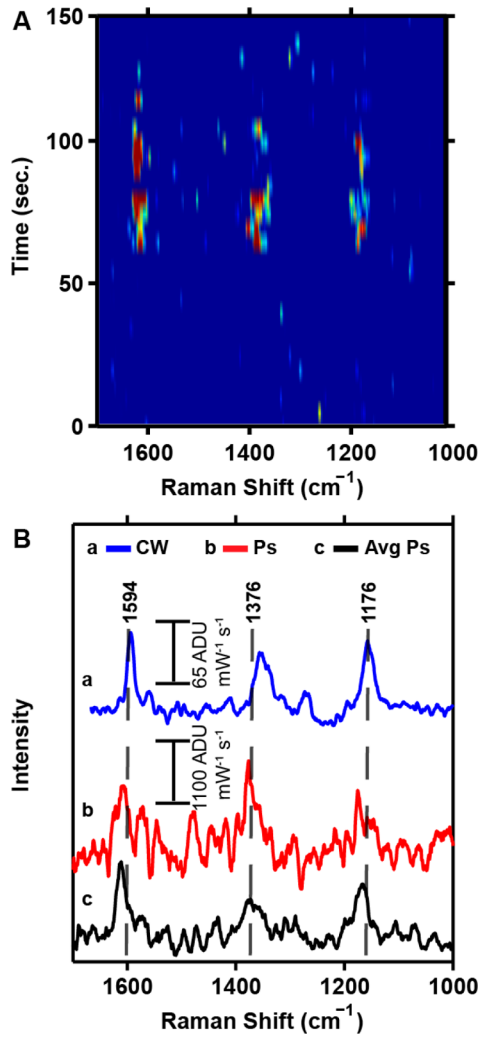


**Figure 2.** (A) Time series waterfall plot of CV, demonstrating the disappearance of the TER signal under pulsed excitation. The disappearance occurs within 40 s after the tip is engaged at $t$ = 60 s. (B) Comparison of pulsed excitation as compared with the signal that can be achieved with CW excitation. Ps TERS spectra acquired with $\lambda_{ex}$ = 594 nm, $t_{aq}$ = 5 s, and $P_{ex}$ = 30 W/cm$^2$ and tunneling conditions of 3 nA and 500 mV. CW TERS spectra acquired with $\lambda_{ex}$ = 594 nm, $t_{aq}$ = 5 s, and average $P_{ex}$ = $10^3$ W/cm$^2$.

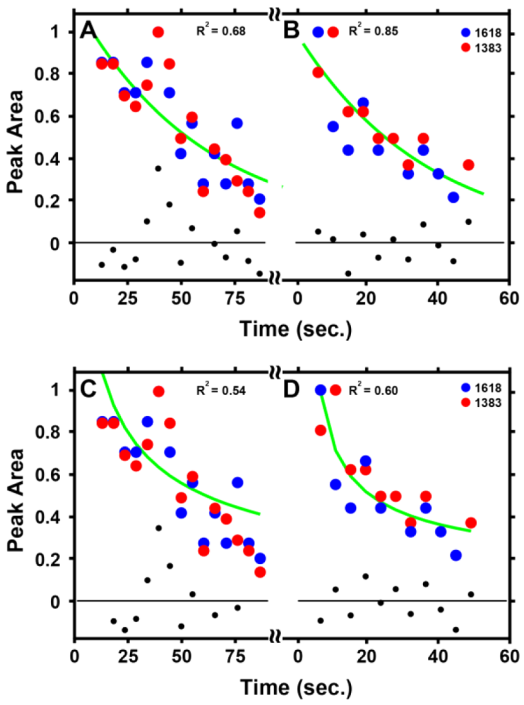


**Figure 3.** Plot of the time dependence of the integrated intensity of the 1618 (blue) and 1383 (red) cm$^{-1}$ bands of MGITC shown in Figure 1A. The areas are normalized to the highest value, and only those above the noise are plotted. The break indicates moving the tip to a new position within the laser focus. The fits to the data in (A,B) exponential ($e^{-k/\tau}$) and (C,D) inverse square root ($t^{-1/2}$) are plotted in green, while the residuals are plotted in gray and $R^2$ values are shown for each case.

is 100 times higher than the average power densities used in the CW experiments. Another possible source of signal decrease could be thermal drift in the STM. We view this as unlikely given that a full monolayer of MGITC is chemisorbed on the surface. Signal loss from thermal drift onto a bare region of the surface is therefore discounted. After observing the signal decay, the TER signal can be fully recovered by repositioning the tip to a different location within the far-field excitation area (Figure 3B,D). Additionally, illumination of the tip while out of tunneling conditions (for CV) did not prevent the TER signal from being observed once the tip was engaged indicating that the signal loss is not a result of tip damage. The most likely explanation for the TERS signal decay is the high peak power density of the OPO tightly focused on the tip−sample junction combined with the ∼100-fold enhancement of the incident electromagnetic field.

The mechanism of signal decay can be interrogated by fitting the decay curves to a variety of functions to examine possible decay pathways. Figure 3A−D shows the decay of the integrated intensity of two of the peaks (1383 and 1618 cm$^{-1}$) present in MGITC. The left decay curve is obtained at one position within the laser focus. After the signal has vanished, the tip was moved to a new spot within the laser focal area and brought into tunneling range. The TER signal returned before similar intensity loss was observed as shown in the right decay curve. TER signal decay for MGITC on Au(111) under 0.5 mW of 633 nm CW excitation has been reported and fit to an exponential with a time constant of 7.3 s.[26] In our experiments, the observed rate of signal decrease is similar across two peaks in MGITC and for two surface sites, indicating that the mechanism is independent of the molecule of interest.

The functional form of the signal loss is consistent with first-order kinetics ($e^{-t/\tau}$) and not with surface diffusion ($t^{-1/2}$). The exponential fits result in time constants $\tau$ = 64 and 43 s for the left and right curves, respectively. The signal fluctuations, much larger than the noise, are the reason the two data sets have different time constants. Given the calculated time constants, we are observing only one lifetime of the decay process, and more mechanistic information would be accessible if it were possible to observe the decay over three to five lifetimes. This analysis suggests several plausible decay mechanisms: (1) irreversible degradation (photochemical or photothermal); (2) reactive decay chemistry between excited dye molecules and $O_2$ or $H_2O$ in the ambient environment; (3) photothermal desorption; and (4) surface diffusion away from the tip (viz., a heated point source). The irreversible degradation mechanism for signal loss is unlikely, as no new Raman lines or carbonaceous background signal (broad peaks at ∼1350 and


dx.doi.org/10.1021/jz4024404 | J. Phys. Chem. Lett. 2014, 5, 106−110

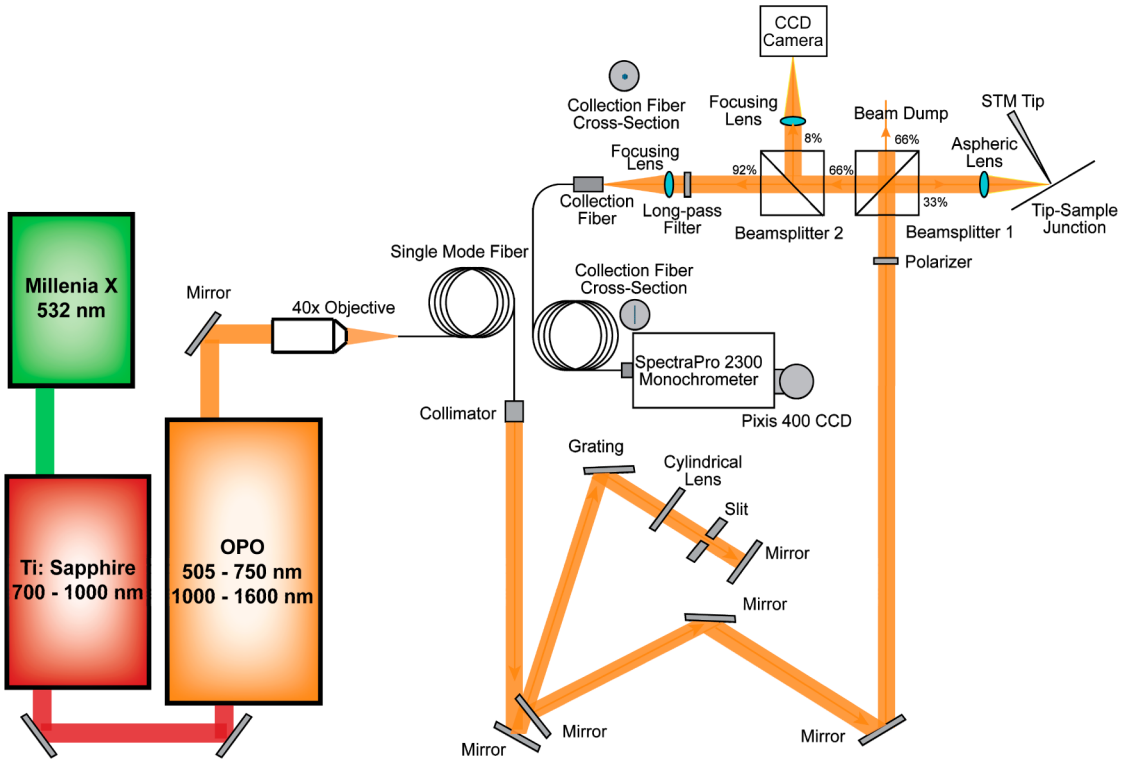


**Figure 4.** Schematic of the experimental setup for picosecond pulsed excitation consisting of a home-built optical microscope, tunable laser system, and a commercial STM.

~1550 $cm^{-1}$) grow into the spectra. Surface diffusion away from the tip is also unlikely as MGITC is covalently attached to the surface. The most likely decay mechanisms are reactive decay and photothermal desorption, both of which are consistent with first-order kinetics. Our intent is to perform experiments with picosecond excitation in UHV that will allow us to rule in or out reactive decay due to the presence of $H_2O$ and $O_2$. Additionally, UHV conditions can definitively eliminate molecular decomposition and surface diffusion as possible decay mechanisms via direct STM imaging.

In summary, TER spectra have been obtained using picosecond pulses. These results clearly demonstrate that it is possible to couple ultrafast spectroscopy to TERS, albeit with a decay problem to be solved or, at least, managed. We have demonstrated that the plasmonic TERS probe is not damaged and that stable tunneling current can be achieved with picosecond excitation of the plasmonic tip. Additionally, TER signal decay was only observed for the molecules in the tip–sample junction. This is most likely due to the combination of high pulse intensity and the intense plasmonic enhancement generated directly under the tip apex. Molecular decomposition does not appear to be responsible for the signal loss, as no new Raman lines or background grow in as the TER signal decays. Molecules not in the enhancing region but still within the far-field laser focus showed no observable decay. Utilizing more robust analytes, such as inorganic coordination complexes, performing experiments in the UHV environment to eliminate $O_2$ and $H_2O$ and using even lower power densities enabled by sharper tips are three promising approaches to solving the decay problem. The coupling of ultrafast spectroscopy will allow TERS to achieve high temporal resolution along with nanometer spectroscopic and submolecular topographic resolution, providing a powerful new tool to study site-specific chemistry occurring at a surface with sensitivity potentially reaching the single-molecule level.

## EXPERIMENTAL METHODS

*Instrumentation.* The STM is identical to that shown previously.[8] A schematic of the Raman microscope is shown in Figure 4. Excitation at the tip–sample junction was achieved through a laser system that is continuously tunable from 500 to 1600 nm via a synchronously pumped intracavity doubled optical parametric oscillator (Coherent Mira-OPO) pumped by a Ti:sapphire mode-locked oscillator (Spectra Physics Tsunami) and a continuous wave 532 nm diode-pumped solid-state laser (Spectra Physics Millenia). The repetition rate of the laser is 80 MHz with pulses on the order of 1 ps in length. The OPO was tuned to 594 nm and was launched through a single-mode fiber before being spectrally dispersed (Thorlabs 1800 g/mm) to remove any Raman light generated in the fiber before entering the optical microscope. The tip approach, tunneling parameters, and feedback were operated by a commercial STM system (Molecular Imaging) controlled by RHK electronics (SPM-100). The experimental conditions are: $\lambda_{ex}$ = 594 nm, incident power density ($P_{ex}$) = 30 W/$cm^2$, $t_{acq}$ = 5 s, bias (V) = 500 mV, and tunneling current ($I_c$) = 3 nA.

*Sample Preparation.* The Ag tips used in this experiment were prepared through electrochemical etching similar to the method described by Zhang et al.[5] The tips were rinsed with Milli-Q water, followed by ethanol after etching. Smooth silver films were prepared by electron beam deposition (AXXIS, Kurt J. Lesker) of 200 nm of silver at a rate of 2 Å/s onto a piranha-cleaned glass coverslip. The films were incubated in a $3 \times 10^{-4}$ M ethanolic solution of either CV or MGITC for at least 4 h and rinsed with ethanol to achieve monolayer coverage.


dx.doi.org/10.1021/jz4024404 | J. Phys. Chem. Lett. 2014, 5, 106–110

## ■ ASSOCIATED CONTENT

### Supporting Information

Absorbance data and time series of TERS with continuous wave excitation for both MGITC and CV. This material is available free of charge via the Internet at http://pubs.acs.org.

## ■ AUTHOR INFORMATION


### Corresponding Author

*E-mail: vanduyne@northwestern.edu.

### Author Contributions

†J.M.K. and M.D.S. contributed equally.


### Notes

The authors declare no competing financial interest.

## ■ ACKNOWLEDGMENTS

This research was made possible by the unique opportunities granted by the NSF Center for Chemical Innovation dedicated to Chemistry at the Space-Time Limit (CHE-082913). Additional support was provided by the National Science Foundation (CHE-1152547 and DMR-1121262) and the Department of Energy Basic Energy Sciences (DE-FG02-09ER16109).

## ■ REFERENCES


(1) Seo, J.; Kim, W. J.; Kim, S. J.; Lee, K.-S.; Cartwright, A. N.; Prasad, P. N. Polymer Nanocomposite Photovoltaics Utilizing Cdse Nanocrystals Capped with a Thermally Cleavable Solubilizing Ligand. *Appl. Phys. Lett.* **2009**, *94*, 133302/1−133302/3.

(2) Opilik, L.; Bauer, T.; Schmid, T.; Stadler, J.; Zenobi, R. Nanoscale Chemical Imaging of Segregated Lipid Domains Using Tip-Enhanced Raman Spectroscopy. *Phys. Chem. Chem. Phys.* **2011**, *13* (21), 9978−9981.

(3) Stadler, J.; Schmid, T.; Zenobi, R. Nanoscale Chemical Imaging of Single-Layer Graphene. *ACS Nano* **2011**, *5*, 8442−8448.

(4) van Schrojenstein Lantman, E. M.; Deckert-Gaudig, T.; Mank, A. J. G.; Deckert, V.; Weckhuysen, B. M. Catalytic Processes Monitored at the Nanoscale with Tip-Enhanced Raman Spectroscopy. *Nat. Nanotechnol.* **2012**, *7*, 583−586.

(5) Zhang, W.; Yeo, B. S.; Schmid, T.; Zenobi, R. Single Molecule Tip-Enhanced Raman Spectroscopy with Silver Tips. *J. Phys. Chem. C* **2007**, *111* (4), 1733−1738.

(6) Steidtner, J.; Pettinger, B. Tip-Enhanced Raman Spectroscopy and Microscopy on Single Dye Molecules with 15 nm Resolution. *Phys. Rev. Lett.* **2008**, *100* (23), 236101/1−236101/4.

(7) Liu, Z.; Ding, S. Y.; Chen, Z. B.; Wang, X.; Tian, J. H.; Anema, J. R.; Zhou, X. S.; Wu, D. Y.; Mao, B. W.; Xu, X.; et al. Revealing the Molecular Structure of Single-Molecule Junctions in Different Conductance States by Fishing-Mode Tip-Enhanced Raman Spectroscopy. *Nat. Commun.* **2011**, *2*, 1−6.

(8) Sonntag, M. D.; Klingsporn, J. M.; Garibay, L. K.; Roberts, J. M.; Dieringer, J. A.; Seideman, T.; Scheidt, K. A.; Jensen, L.; Schatz, G. C.; Van Duyne, R. P. Single-Molecule Tip-Enhanced Raman Spectroscopy. *J. Phys. Chem. C* **2012**, *116* (1), 478−483.

(9) Zhang, R.; Zhang, Y.; Dong, Z.; Jiang, S.; Zhang, C.; Chen, L.; Zhang, L.; Liao, Y.; Aizpurua, J.; Luo, Y. Chemical Mapping of a Single Molecule by Plasmon-Enhanced Raman Scattering. *Nature* **2013**, *498* (7452), 82−86.

(10) Stadler, J.; Oswald, B.; Schmid, T.; Zenobi, R. Characterizing Unusual Metal Substrates for Gap-Mode Tip-Enhanced Raman Spectroscopy. *J. Raman Spectrosc.* **2013**, *44* (2), 227−233.

(11) Jiang, N.; Foley, E. T.; Klingsporn, J. M.; Sonntag, M. D.; Valley, N. A.; Dieringer, J. A.; Seideman, T.; Schatz, G. C.; Hersam, M. C.; Van Duyne, R. P. Observation of Multiple Vibrational Modes in Ultrahigh Vacuum Tip-Enhanced Raman Spectroscopy Combined with Molecular-Resolution Scanning Tunneling Microscopy. *Nano Lett.* **2012**, *12* (10), 5061−5067.

(12) Dolocan, A.; Acharya, D. P.; Zahl, P.; Sutter, P.; Camillone, N. Two-Color Ultrafast Photoexcited Scanning Tunneling Microscopy. *J. Phys. Chem. C* **2011**, *115* (20), 10033−10043.

(13) Dombi, P.; Hörl, A.; Rácz, P.; Márton, I.; Trügler, A.; Krenn, J. R.; Hohenester, U. Ultrafast Strong-Field Photoemission from Plasmonic Nanoparticles. *Nano Lett.* **2013**, *13* (2), 674−678.

(14) Takeuchi, O.; Aoyama, M.; Oshima, R.; Okada, Y.; Oigawa, H.; Sano, N.; Shigekawa, H.; Morita, R.; Yamashita, M. Probing Subpicosecond Dynamics Using Pulsed Laser Combined Scanning Tunneling Microscopy. *Appl. Phys. Lett.* **2004**, *85* (15), 3268−3270.

(15) Dey, S.; Mirell, D.; Perez, A. R.; Lee, J.; Apkarian, V. A. Nonlinear Femtosecond Laser Induced Scanning Tunneling Microscopy. *J. Chem. Phys.* **2013**, *138* (15), 154202/1−154202/10.

(16) Neacsu, C. C.; van Aken, B. B.; Fiebig, M.; Raschke, M. B. Second-Harmonic near-Field Imaging of Ferroelectric Domain Structure of $YMnO_3$. *Phys. Rev. B* **2009**, *79* (10), 100107/1−100107/4.

(17) Ropers, C.; Solli, D. R.; Schulz, C. P.; Lienau, C.; Elsaesser, T. Localized Multiphoton Emission of Femtosecond Electron Pulses from Metal Nanotips. *Phys. Rev. Lett.* **2007**, *98* (4), 043907/1−043907/4.

(18) Bormann, R.; Gulde, M.; Weismann, A.; Yalunin, S. V.; Ropers, C. Tip-Enhanced Strong-Field Photoemission. *Phys. Rev. Lett.* **2010**, *105* (14), 147601/1−147601/4.

(19) Berweger, S.; Atkin, J. M.; Xu, X. G.; Olmon, R. L.; Raschke, M. B. Femtosecond Nanofocusing with Full Optical Waveform Control. *Nano Lett.* **2011**, *11*, 4309−4313.

(20) Ichimura, T.; Hayazawa, N.; Hashimoto, M.; Inouye, Y.; Kawata, S. Tip-Enhanced Coherent Anti-Stokes Raman Scattering for Vibrational Nanoimaging. *Phys. Rev. Lett.* **2004**, *92*, 220801/1−220801/4.

(21) Furusawa, K.; Hayazawa, N.; Catalan, F. C.; Okamoto, T.; Kawata, S. Tip-Enhanced Broadband CARS Spectroscopy and Imaging Using a Photonic Crystal Fiber Based Broadband Light Source. *J. Raman Spectrosc.* **2012**, *43*, 656−661.

(22) Sung, J.; Kosuda, K. M.; Zhao, J.; Elam, J. W.; Spears, K. G.; Van Duyne, R. P. Stability of Silver Nanoparticles Fabricated by Nanosphere Lithography and Atomic Layer Deposition to Femtosecond Laser Excitation. *J. Phys. Chem. C* **2008**, *112*, 5707−5714.

(23) Frontiera, R. R.; Henry, A.-I.; Gruenke, N. L.; Van Duyne, R. P. Surface-Enhanced Femtosecond Stimulated Raman Spectroscopy. *J. Phys. Chem. Lett.* **2011**, *2*, 1199−1203.

(24) Hulteen, J. C.; Young, M. A.; Van Duyne, R. P. Surface-Enhanced Hyper-Raman Scattering (SEHRS) on Ag Film over Nanosphere (FON) Electrodes: Surface Symmetry of Centrosymmetric Adsorbates. *Langmuir* **2006**, *22* (25), 10354−10364.

(25) Milojevich, C. B.; Silverstein, D. W.; Jensen, L.; Camden, J. P. Surface-Enhanced Hyper-Raman Scattering Elucidates the Two-Photon Absorption Spectrum of Rhodamine 6G. *J. Phys. Chem. C* **2013**, *117* (6), 3046−3054.

(26) Pettinger, B.; Ren, B.; Picardi, G.; Schuster, R.; Ertl, G. Tip-Enhanced Raman Spectroscopy (TERS) of Malachite Green Isothiocyanate at Au(111): Bleaching Behavior under the Influence of High Electromagnetic Fields. *J. Raman Spectrosc.* **2005**, *36*, 541−550.